Atmos. Chem. Phys., 10, 7709–7722, 2010
www.atmos-chem-phys.net/10/7709/2010/
doi:10.5194/acp-10-7709-2010

Atmospheric Chemistry and Physics

Evaluation of simulated aerosol properties with the aerosol-climate model ECHAM5-HAM using observations from the IMPACT field campaign

G.-J. Roelofs[1], **H. ten Brink**[2], **A. Kiendler-Scharr**[3], **G. de Leeuw**[4,5,6], **A. Mensah**[3], **A. Minikin**[7], **and R. Otjes**[2]

[1]Institute for Marine and Atmospheric Research Utrecht (IMAU), Utrecht University, Princetonplein 5, 3584 CC Utrecht, The Netherlands
[2]Energy Center Netherlands (ECN), Petten, The Netherlands
[3]ICG-2: Troposphere, Forschungszentrum Jülich GmbH, Germany
[4]Business unit Environment, Health and Safety, TNO, Utrecht, The Netherlands
[5]Finnish Meteorological Institute, Climate Change Unit, Helsinki, Finland
[6]University of Helsinki, Department of Physics, Helsinki, Finland
[7]Deutsches Zentrum für Luft- und Raumfahrt (DLR), Oberpfaffenhofen, Germany

Received: 27 January 2010 – Published in Atmos. Chem. Phys. Discuss.: 1 March 2010
Revised: 14 July 2010 – Accepted: 20 July 2010 – Published: 19 August 2010

Abstract. In May 2008, the measurement campaign IMPACT for observation of atmospheric aerosol and cloud properties was conducted in Cabauw, The Netherlands. With a nudged version of the coupled aerosol-climate model ECHAM5-HAM we simulate the size distribution and chemical composition of the aerosol and the associated aerosol optical thickness (AOT) for the campaign period. Synoptic scale meteorology is represented realistically through nudging of the vorticity, the divergence, the temperature and the surface pressure. Simulated concentrations of aerosol sulfate and organics at the surface are generally within a factor of two from observed values. The monthly averaged AOT from the model is 0.33, about 20% larger than observed. For selected periods of the month with relatively dry and moist conditions discrepancies are approximately −30% and +15%, respectively. Discrepancies during the dry period are partly caused by inaccurate representation of boundary layer (BL) dynamics by the model affecting the simulated AOT. The model simulates too strong exchange between the BL and the free troposphere, resulting in weaker concentration gradients at the BL top than observed for aerosol and humidity, while upward mixing from the surface layers into the BL appears to be underestimated. The results indicate that beside aerosol sulfate and organics also aerosol ammonium and nitrate significantly contribute to aerosol water uptake. The simulated day-to-day variability of AOT follows synoptic scale advection of humidity rather than particle concentration. Even for relatively dry conditions AOT appears to be strongly influenced by the diurnal cycle of RH in the lower boundary layer, further enhanced by uptake and release of nitric acid and ammonia by aerosol water.

Correspondence to: G. J. Roelofs
(g.j.h.roelofs@uu.nl)

1 Introduction

Aerosol particles directly scatter part of the solar radiation back to space, and in addition they influence cloud optical characteristics and cloud lifetime through the so-called first and second aerosol indirect effects (e.g., Lohmann and Feichter, 2005). Anthropogenic activities have caused an increase of the atmospheric burden of aerosol and aerosol precursors compared to the pre-industrial atmosphere, and this may have altered regional and global radiative cloud forcing (e.g., Forster et al., 2007). The large spatial and temporal variability in size, chemical composition, and hygroscopicity of particles impede accurate estimation of the aerosol direct and indirect forcing (Textor et al., 2006) and lead to large uncertainties in assessing the sensitivity of climate to human perturbations and in projections of climate change (Andreae et al., 2005).

Published by Copernicus Publications on behalf of the European Geosciences Union.

To estimate the magnitude of the radiative forcing due to aerosol direct and indirect effects, coupled aerosol-climate models that simulate activation of aerosol to cloud droplets can be applied (Lohmann et al., 2007; Penner et al., 2006). Due to the complexity of aerosol processes and inaccuracies in the representation of the hydrological cycle, current model estimates of the radiative forcing display a large range, between -0.2 and $-0.9\,\mathrm{W\,m^{-2}}$ for the direct effect and between -0.5 and $-1.5\,\mathrm{W\,m^{-2}}$ for the indirect effect (Forster et al., 2007; Quaas et al., 2009). Analysis of aerosol properties retrieved from satellite measurements may help to decrease current uncertainties in aerosol burden and global distribution (e.g., Kaufman et al., 2002). Retrieved aerosol optical thickness (AOT) is assumed to indicate the aerosol column burden while the Angström exponent can be used to estimate the fine fraction of the aerosol, often associated with the anthropogenic contribution (Kaufman et al., 2005; Anderson et al., 2005). Estimates of the aerosol climate forcing based on satellite retrieval are -0.8±0.1 $\mathrm{W\,m^{-2}}$ (Bellouin et al., 2005) and $-0.9\pm0.4\,\mathrm{W\,m^{-2}}$ (Quaas et al., 2008) for the direct effect, and $-0.2\pm0.1\,\mathrm{W\,m^{-2}}$ for the indirect effect (Quaas et al., 2008). Satellite based aerosol retrievals are characterized by considerable uncertainties associated for example with surface albedo or cloud contamination, but the inconsistency between model and remote sensing estimates may also be due to the model representation of aerosol and cloud processes (Quaas et al., 2009) or the uncertain influence of black carbon (Myhre et al., 2009). Other reasons are associated with relative humidity (RH). These are the nonlinear swelling of hygroscopic aerosol through water uptake especially for RH larger than ∼80% (Schuster et al., 2006), the influence of cloud processing on AOT and Angström exponent (Roelofs and Kamphuis, 2009), and the influence of RH and its sub-grid scale variability (Bian et al., 2009; Jeong et al., 2007).

In this study we simulate atmospheric aerosol and AOT in May 2008, with the coupled aerosol-climate model ECHAM5-HAM. The model contains a size-resolved representation of aerosol and different aerosol components, and a sophisticated aerosol activation and cloud chemistry parameterization. The purpose of the study is to validate simulated aerosol properties and AOT, and to investigate the contribution of different parameters (particle concentrations, chemical composition and RH) on the column integrated AOT. For the validation of aerosol parameters we use measurements obtained during the IMPACT campaign in May 2008 (Intensive Measurement campaign at Cabauw Tower) (Cabauw, The Netherlands, 51°58′ N, 4°54′ E). IMPACT was conducted as part of EUCAARI (European Integrated Project on Aerosol Cloud Climate Air Quality Interactions), a European project aimed to reduce uncertainties associated with aerosol climate effects and to quantify the impact on climate of air quality directives in Europe. Measurements were conducted at the surface, from a 200 m measurement tower, with balloon sondes and from a helicopter and from aircraft. These resulted in detailed information on meteorological parameters, aerosol size-distribution and chemical composition, atmospheric trace gases, radiative fluxes and cloud parameters. For more information on EUCAARI we refer to the overview paper by Kulmala et al. (2009). For AOT we use values from the Aerosol Robotic Network (AERONET, http://aeronet.gsfc.nasa.gov/). AERONET is a worldwide net of ground-based remote sensing of aerosol that provides observations of spectral AOT and several inversion products.

Section 2 of this manuscript provides a description of the coupled aerosol-climate model. Section 3 presents a comparison of observed and simulated meteorological parameters and aerosol optical and chemical properties in May 2008 at Cabauw. In Sect. 4 three characteristic episodes in this month are discussed in more detail. Section 5 presents a summary of the results and conclusions.

2 Model description

We use a version of the coupled aerosol-climate model ECHAM5-HAM similar to the one applied by Stier et al. (2005). ECHAM5-HAM consists of the general circulation model ECHAM version 5 and an aerosol module (HAM). The model uses 19 vertical layers in a hybrid σ-p-coordinate system, from the surface to 10 hPa. Average pressure levels in the troposphere are 990, 970, 950, 900, 840, 760, 670, 580, 490, 400, 320 and 250h Pa, referring to approximate mid-layer altitudes of 0.03, 0.14, 0.38, 0.78, 1.4, 2.1, 3.1, 4.2, 5.6, 7.0, 8.6 and 10.2 km above the surface, respectively. The model resolution is T63, corresponding with a horizontal resolution of ∼1.8° (∼120 km at 52° N) and a time resolution of 15 minutes. The meteorology is nudged with ECMWF 6hourly spectral analysis data for vorticity, divergence, temperature and surface pressure, starting from January 2008. The parameters are used by ECHAM5 to compute actual wind fields. Further, atmospheric water vapor is not nudged but follows directly from the simulation of the atmospheric hydrological cycle.

HAM accounts for emissions of primary aerosol and aerosol precursors, chemical transformations, nucleation of new particles and condensation of semi-volatile H_2SO_4 on existing particles, coalescence between particles and dry and wet deposition. The core of HAM is the aerosol dynamical module M7 (Vignati et al., 2004; Wilson et al., 2001). M7 describes the aerosol population with four soluble and three insoluble aerosol modes composed of (mixtures of) sulfate, organic carbon, black carbon, sea salt and dust. The modes are described as lognormal distributions of particle concentrations, and each mode is characterized by the total particle number concentration and mass of associated aerosol components. The size ranges considered are below 0.005 µm dry particle radius for the nucleation mode, between 0.005 and 0.05 µm dry particle radius for the Aitken mode, between 0.05 and 0.5 µm dry particle radius for the

accumulation mode, and above 0.5 µm dry particle radius for the coarse mode. The model considers emissions of the aerosol precursor gas SO_2 and dimethyl sulfide, and calculates sulfate formation in the gaseous and aqueous phase using offline oxidant fields. All other emissions are treated as primary. Also, formation of secondary organic aerosol (SOA) is not calculated explicitly but all organics are emitted as primary particles. The molecular weight of oxalic acid is taken to be representative for the organic matter, and the organics are distributed evenly over the soluble and insoluble aerosol modes. The organics in the soluble aerosol are assumed to have a soluble fraction of 50% while surface tension effects are neglected. The emissions of dust, sea salt, dimethyl sulfide and marine organics are calculated online (Stier et al., 2005; Roelofs, 2008). The emissions of other aerosol compounds are based on the AEROCOM emission inventory and representative for the year 2000 (Dentener et al., 2006). In the Cabauw grid point anthropogenic emissions dominate, with 1.5×10^{-10} kg S m^{-2} s^{-1} and 3.0×10^{-11} kg organic C m^{-2} s^{-1}.

The bulk cloud chemistry scheme in ECHAM5-HAM has been replaced with a cloud processing parameterization (Roelofs et al., 2006). First, the cloud drop number concentration is estimated through an empirical approach. The second step in the parameterization calculates aqueous phase formation of sulfate and its distribution over the different activated modes, i.e., the modes that contribute to the cloud drop number concentration. The parameterization is linked to the climate model's large-scale cloud scheme (Lohmann and Roeckner, 1996). In the current study the cloud droplet concentration is not coupled to the calculation of precipitation formation and cloud optical properties, implying that aerosol indirect effects are not considered.

North-West Europe is characterized by relatively high concentrations of nitric acid and ammonia (e.g., Myhre et al., 2006). Our model does not consider aerosol chemistry associated with nitric acid and ammonia, although a prescribed aerosol ammonium concentration results from our assumption that half of the computed sulfate amount is immediately neutralized by ammonium. We implemented a simple equilibrium dissolution and dissociation module for nitric acid, which is considered on the Cabauw grid point for AOT calculations only. A HNO_3 gas phase concentration in the boundary layer of 3 ppb is prescribed, which corresponds to the sum of the observed HNO_3 and aerosol nitrate concentrations of $\sim$8 µg/m^3.

The AOT calculations are based on the simulated modal masses of the individual aerosol components and the particle number concentration for each mode. These are used to calculate the median dry particle radius, and for the soluble modes also the median wet radius. In the standard model version the wet radius is calculated from the simulated aerosol sulfate and sea salt burdens (Vignati et al., 2004). In the present study we employ a more versatile approach based on the Koehler equation that considers also ammonium, nitrate, hydrogen ions and soluble organic matter. Each simulated aerosol species is associated with a complex refractive index that is used for calculating its optical properties based on Mie theory (see Stier et al., 2005).

3 Results

3.1 Meteorological and aerosol parameters

Figure 1 shows the distribution of simulated AOT over Europe for the periods 6–11, 12–16, 17–22 and 23–31 May. The location of Cabauw is indicated. According to the model, the Netherlands, Germany, Denmark and southern Scandinavia were characterized by relatively small AOT between 6–11 May, on average below 0.2, while AOT over the south of Europe and the United Kingdom was larger, between 0.5–0.9. Between 12–16 May a band of relatively high AOT is situated over The Netherlands and southern part of the United Kingdom, with AOT values over the Netherlands and Germany ranging between 0.4 and 0.9. Between 17–22 May relatively clean marine air is advected into The Netherlands from the north, and AOT over Cabauw is smaller again. In the last week of the month, between 23 and 31 May, simulated AOT over Cabauw is relatively large, $\sim$1.4. This is associated with a combined influence of European pollution stretching in a latitudinal band at 52° N between 4° W and 20° E and desert dust from the Sahara that is advected northward between 4° E and 10° E.

Figure 2 shows AOT and the Angström exponent from AERONET at Cabauw in May 2008. We transformed the measurements for 440 nm by means of the observed Angström exponent to 553 nm, the wavelength employed by ECHAM. We included data from level 1.5 (cloud-screened) as well as from level 2.0 (cloud-screened and quality assured). Figure 2 also shows simulation results filtered for cloudy conditions, i.e., the simulated grid point-averaged liquid water and ice columns combined do not exceed a threshold of 0.05 g/m^2. The figure shows that for this threshold the simulation data are more consistent with the L1.5 than with the L2.0 AERONET data, for example on 17 May but especially after 24 May when the atmosphere above Cabauw contains relatively large quantities of Sahara dust. It is possible that in the quality assurance procedure these AERONET data were associated with cloudy conditions and consequently excluded. Because of the higher consistency with the simulation results we will consider the AERONET L1.5 data in the remainder of this study. The estimated uncertainty of AOT from AERONET is $\pm$0.02 (Eck et al., 2005).

It must be remarked that a comparison between grid-averaged simulation results and local observations such as presented in this study can be hampered by scale differences between both data sets. The representativity of a comparison depends on the spatial distribution of emissions, on specific lifetimes of trace species for chemical destruction, transport

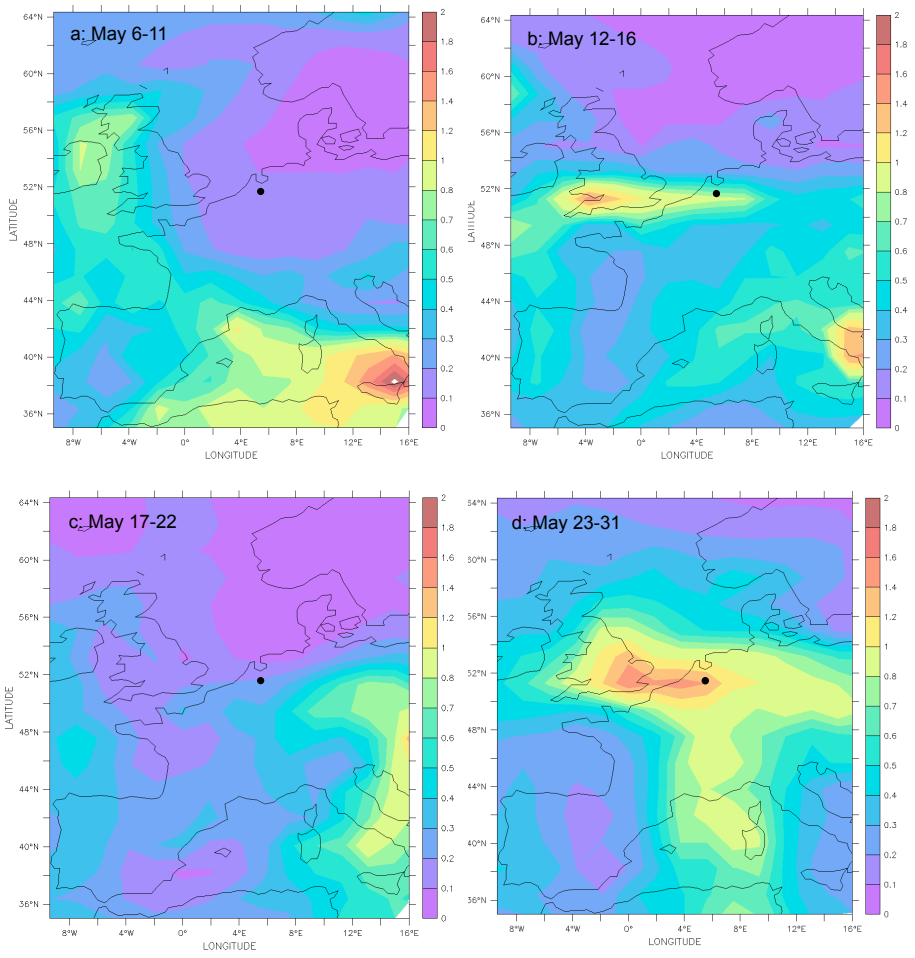

Fig. 1. Simulated AOT averaged over **(a)** 6–11 May; **(b)** 12–16 May; **(c)** 17–22 May and **(d)** 23–31 May. The black dots indicate the location of Cabauw.

and deposition, and on small-scale variabilities in meteorological parameters. The transport time through a grid box in our model is typically on the order of one to a few hours whereas the lifetime of aerosol is on the order of a few days. Therefore, sub-grid scale variabilities in aerosol composition and concentration due to synoptic advection are probably small. Humidity and clouds, on the other hand, may display spatial variabilities on scales smaller than the grid size, especially in the moist second half of the month, which may contribute to any discrepancy between model result and observation.

The simulated time series of AOT and the Angström exponent (AE) are qualitatively consistent with AERONET L1.5 but several discrepancies can be noticed. Between 1–6 May the model situates two relatively narrow dust filaments, remnants of a Saharan dust event that occurred in April 2008, north and south of Cabauw (not shown). Considering the relatively large AOT and highly variable Angström exponent (Fig. 2b) it is possible that on 2 and 3 May one filament was detected above Cabauw by AERONET, but this is not simulated. The other filament influences the Cabauw model grid point on 6 May, with an AOT larger than observed. Between 7–12 May simulated AOT is smaller than observed and does not reproduce the observed diurnal variability. AOT is also underestimated during 18–22 May. Between 13–17 and 23–31 May the model simulates larger AOT, qualitatively consistent with AERONET but about double the observed values during 28–31 May. AE (Fig. 2b) shows considerable scatter in the first four days, followed by relatively high values until 24 May indicating a relatively large fraction of fine mode particles, and relatively small values after 24 May (only in L1.5) indicating a significant coarse mode particle concentration. Simulated AE is of the right order of magnitude between 5–9 May. After that it increases until 12 May rather than decrease as observed. Simulated and observed AE are in better agreement after 18 May.

The average observed AOT (553 nm, L1.5) in May 2008 in Cabauw is 0.275. The average simulated AOT for the cloud filter applied is 0.329, 20% larger than observed. This value is indicative only: for threshold values of 0.01 g/m^2

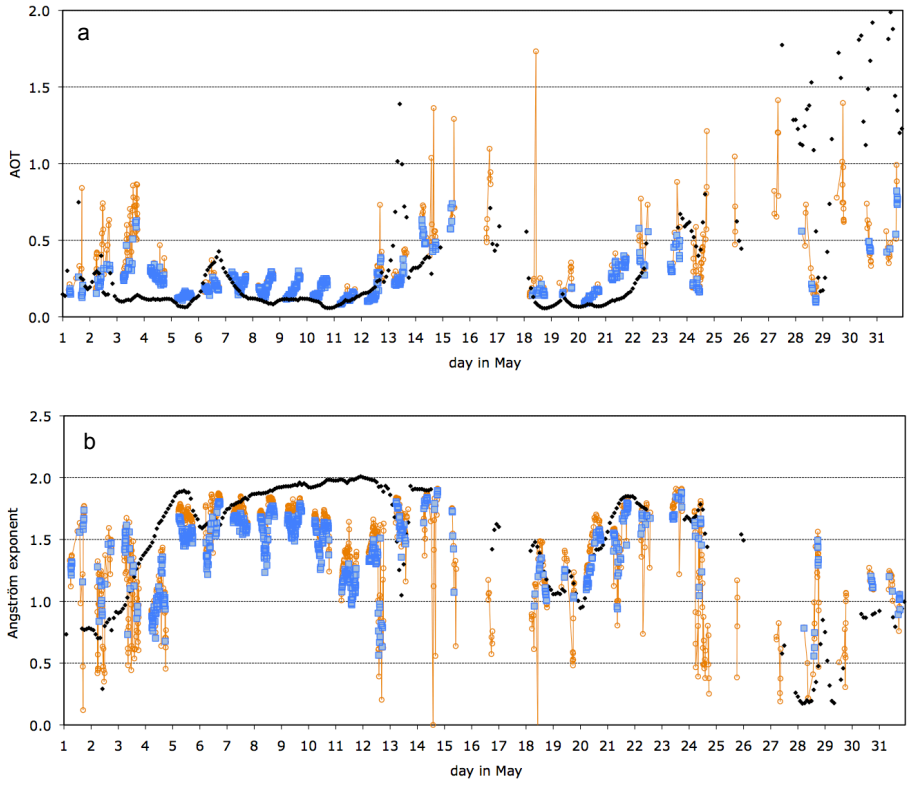

Fig. 2. (a) AOT (553 nm) and **(b)** Angström exponent from the simulation (black) and from AERONET (orange: L1.5; blue: L2.0).

and 0.10 g/m^2 the average AOT is 0.230 and 0.396, respectively. The simulated contributions to AOT (553 nm) by the fine (Aitken and accumulation) and coarse mode fractions are 0.241 and 0.088, respectively, as compared to observed values of 0.180 and 0.095, respectively (not shown).

Figure 2 suggest that the campaign consisted of a sequence of periods with typical AOT values. The individual periods are influenced by the governing wind direction, shown in Fig. 3a, with wind coming from the southeast (2–4 May), from the east (4–12 May), from the northeast and north (13–21 May), and from the east again (22–26 May). Generally, winds coming from a direction between northeast and south advect continental polluted air to Cabauw, and winds coming from the northwest advect cleaner marine air (e.g., Khlystov et al., 1996; Kusmierczyk-Michulec et al., 2007). Between 26–31 May the weather at Cabauw is influenced by an occlusion, leading to rapid variations in wind direction. As a result, a sharp minimum in AOT and maximum of AE occur in the night of 28–29 May (see Fig. 2a), associated with meandering of the dust plume. These are simulated correctly albeit a few hours later than observed. Although the daily variability is underestimated the simulated wind direction at 10m is generally consistent with the observations, except for 1–2 and 29–31 May.

Figure 3b displays measurements from a condensation particle counter (CPC; TSI UCPC 3786) operated by ICG-2 Jülich (http://www.fz-juelich.de/icg/icg-2), and the simulated fine (i.e., Aitken and accumulation) mode particle concentrations. The synoptic variability in observed and simulated concentrations appears similar. During the periods with wind from the east (5–12 and 22–25 May) observed concentrations are about twice the simulated concentration, which is partly due to the different lower size limits in the observations and in the model (3 and 5 nm radius, respectively). The observations display daily peaks up to $\sim$20 000 cm^{-3} in the morning and afternoon, likely associated with efficient photochemical new particle formation. The model qualitatively captures this behaviour. We remark that new particle formation associated with these peaks has been observed in the residual layer as well (Wehner et al., 2010). After 25 May the model simulates a strong concentration increase associated with advection of Saharan dust, while the observations show a similar increase a few days later. The discrepancy is probably associated with the complex meteorology associated with the occlusion. The simulated integrated water vapor (IWV) shown in Fig. 3c agrees relatively well with the observations, although the model tends to overestimate IWV by 10–20%.

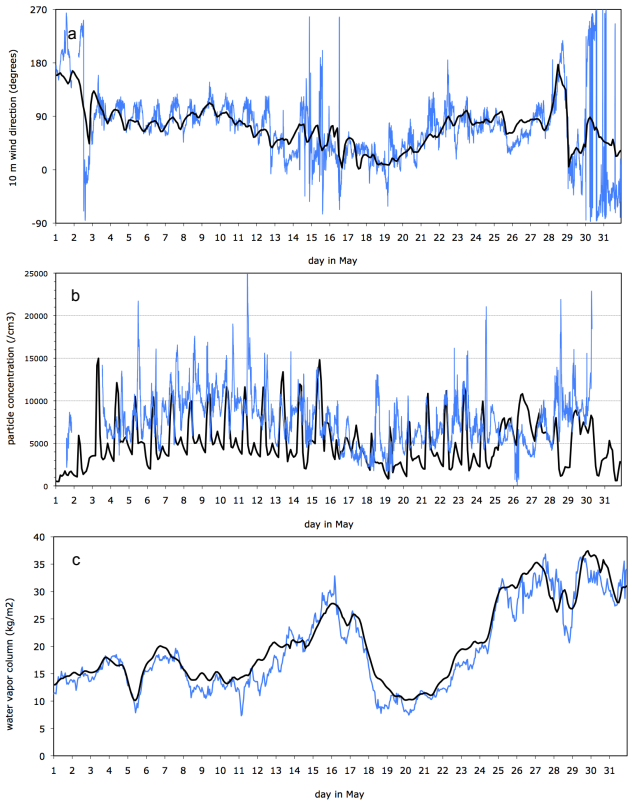

Fig. 3. Observed (blue) and simulated (black) **(a)** 10 m wind direction (degrees), **(b)** surface concentration of fine mode particles(<1 µm diameter; cm^{-3}), and **(c)** water vapor column (IWV, kg/m^2).

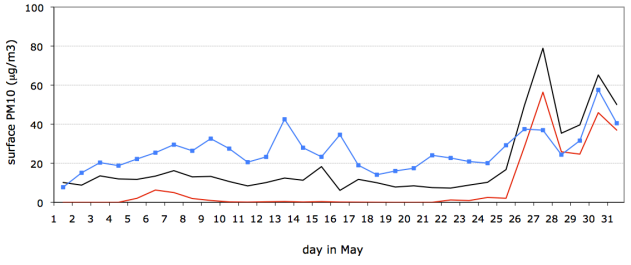

Fig. 4. Observed surface PM_{10} (blue), and simulated daily averages of total aerosol mass (black) and dust mass (red) ($\mu g/m^3$).

3.2 Aerosol physical and chemical properties

Figure 4 shows the simulated total aerosol mass at the surface and the observed PM_{10} (total mass for particle diameter smaller than 10 µm; http://www.lml.rivm.nl/). The simulated aerosol mass is smaller than the observed PM_{10} for most of the month mainly because of underestimation of aerosol nitrate and ammonium, as will be discussed later. The model simulates two periods where dust contributes significantly to the aerosol mass at the surface. The first event occurs around 6 May and has been discussed in Sect. 3.1. The second and largest event occurs between 26–31 May, when Saharan dust contributes ∼70% to the simulated aerosol mass at the surface. Uncertainties in emission, transport and gravitational settling of dust, and possible inconsistencies in the model representation of the relatively complex meteorology over NW Europe on these days may have contributed to the overestimation of aerosol mass at the surface, largest on 26–27 May.

Figure 5 compares simulated and observed masses of aerosol species. Blue dots refer to mass spectrometer measurements from ICG-2 Jülich (Canagaratna et al., 2007). Canagaratna et al. (2007) mention that the lens of the AMS instrument, a PM_1 instrument, offers 100% transmission for particles in the aerodynamic diameter range of 70–500 nm and 50% transmission for particles with 1000 nm diameter. The observations therefore can be considered to reflect the mass contained by particles smaller than 0.56 µm diameter (0.28 µm radius). This corresponds with a subset of the fine mode aerosol in the model, with an upper size limit of 0.5 µm radius. The green dots refer to MARGA-sizer measurements from ECN (Energieonderzoek Centrum Nederland; http://www.ecn.nl) and reflect the total (i.e., fine + coarse mode) mass of the aerosol components.

Figure 5a shows aerosol sulfate concentrations. The calculated order of magnitude is similar as observed, but the model severely overestimates sulfate on 16–17 and 25–28 May. 16–17 May are characterized by a northerly wind that transports cleaner air to Cabauw from the North Sea, and cloudiness. However, in the model Cabauw is located in a land grid with significant emissions of pollutants, a.o. SO_2. These are instantaneously mixed throughout the grid point and influence simulated sulfate levels regardless of wind direction. The overestimate during 25–28 May is probably associated with the overestimation of the atmospheric dust burden (Fig. 4). During its northward transport over the European continent dust interacts with gaseous and particulate pollutants. Deposition of sulfuric acid on the dust surface and coagulation with pollution aerosol may explain the relatively large amounts of sulfate and organic matter.

Observed nitrate concentrations (Fig. 5b) range between 3 and 10 µg/m3 with occasional peaks of 20–30 µg/m3 in relatively moist periods (13–17 May and after 26 May). This suggests that in periods with a high relative humidity the aerosol nitrate uptake by the arosol is significantly enhanced. Simulated concentrations of aerosol nitrate, based on an initial HNO_3 concentration of 3 ppbv, are on the order of 0.7 $\mu g/m^3$. This is negligible compared to the observations although during moist periods simulated aerosol nitrate reaches 3–5 µg/m3. Simulated ammonium concentrations (Fig. 5c) are about half the values observed. The simulated aerosol ammonium directly follows from our assumption that aerosol sulfate is in the form of ammonium bisulfate. The potential role of ammonium and nitrate for AOT will be discussed in more detail in Sect. 4.3.

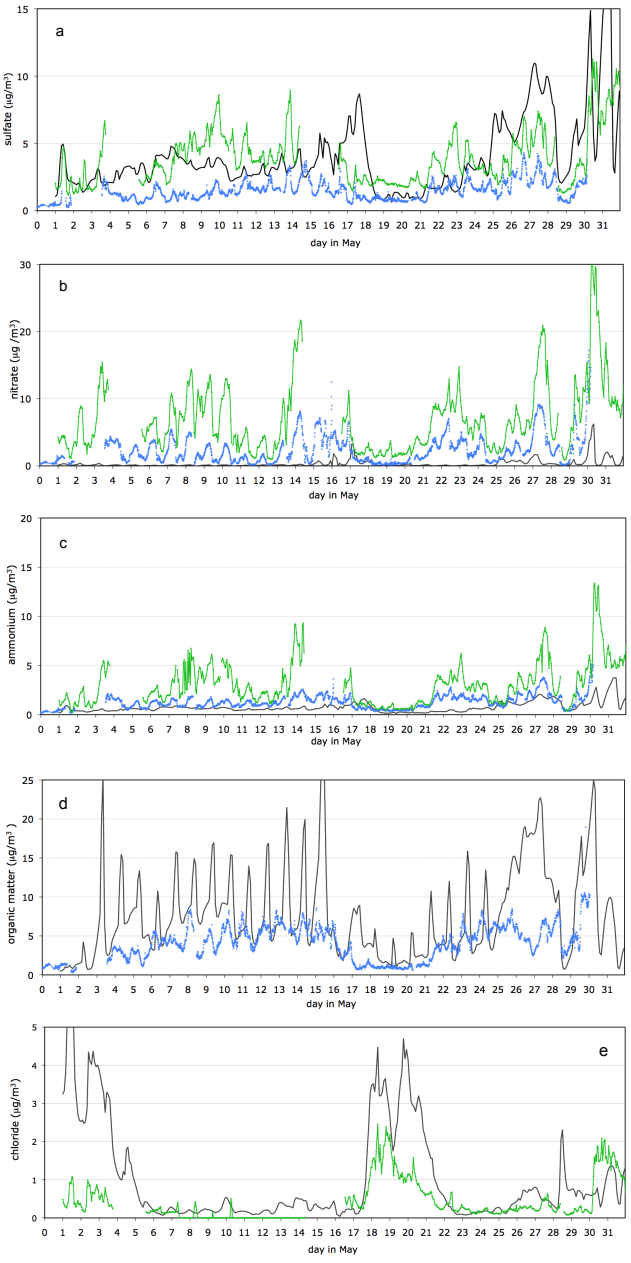

Fig. 5. Observed (blue, green) and simulated (black) concentrations (µg/m^3) of **(a)** sulfate, **(b)** nitrate, **(c)** ammonium, **(d)** organics and **(e)** chloride. Observations are from IMPACT, and simulation results pertain to the Cabauw grid point. Measurements in blue are from ICG-2 Jülich (Germany) and reflect particle sizes <0.56 µm diameter. Measurements in green are from ECN (The Netherlands) and reflect total aerosol mass.

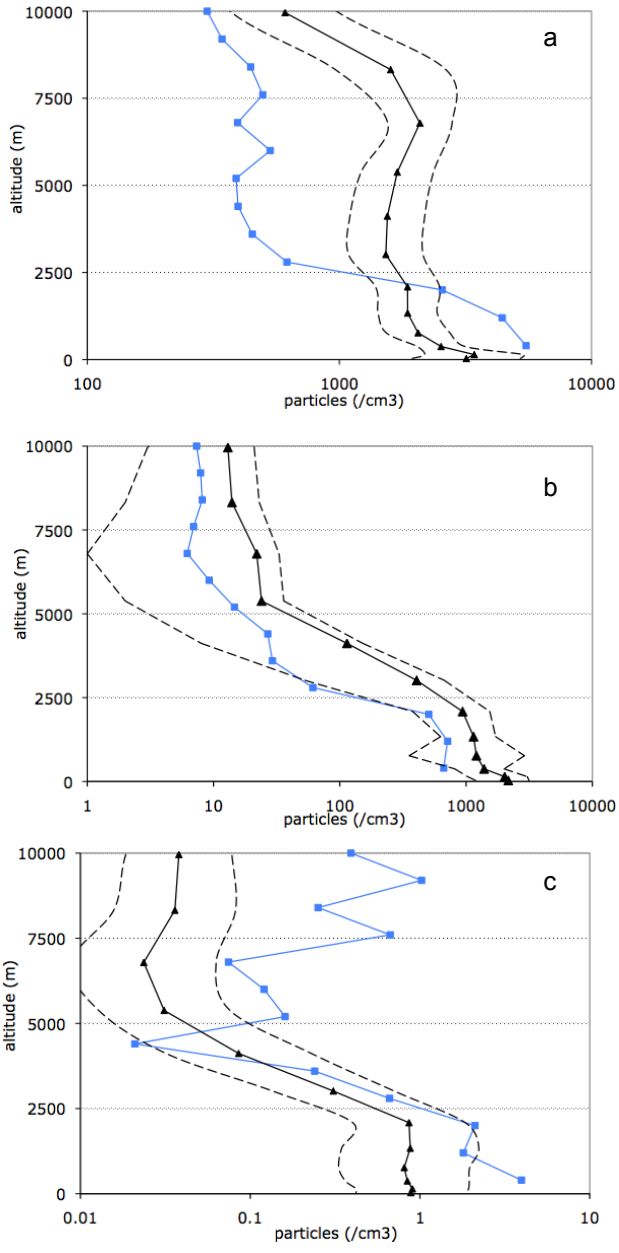

Fig. 6. Observed (blue) and simulated (black) concentration profiles (cm^{-3}) averaged over 2–14 May (daytime) for **(a)** the Aitken mode (size range observations: 10–150 nm diameter; model: 5–50 nm radius), **(b)** the accumulation mode (size range observations: 150–1000 nm diameter; model: 50–500 nm radius), and **(c)** the coarse mode (size range observations: 1–3 µm diameter; model: >0.5 µm radius). Dashed lines reflect the simulated standard deviation.

Simulated daily variability for organic matter (Fig. 5d) is larger than observed due to the fact that the model assumes primary emissions instead of more gradual SOA formation from precursor gases. Nevertheless, on average simulated and observed concentrations agree relatively well. Chloride (Fig. 5e) is almost exclusively found in the coarse mode, and modeled peak concentrations are relatively large compared to the observations. However, both observations and model indicate that the chloride fraction in the aerosol is relatively small during most of the month. We remark that observed chloride concentrations are correlated relatively well with

sodium in a mass concentration ratio of ∼1.5, indicating that chloride is associated with sea salt.

Figure 6 shows simulated and observed particle concentration profiles, averaged over 2–14 May. Simulated values pertain to the Cabauw grid point sampled between 10:00 and 18:00 h (universal time), while the observations reflect aircraft measurements of 10 flights of the DLR Falcon over the Netherlands, Britain and Germany during the same period. These aircraft measurements were part of the EUCAARI-LONGREX campaign conducted during the EUCAARI Intensive Observation Period in 2008. The observed aerosol number concentration profiles in Fig. 6 are based on median values calculated for altitude bins of 800 m, for cloud-free conditions only. Data are based on measurements with a condensation particle counter and two optical aerosol spectrometer probes, a PCASP-100X and a FSSP-300. This instrument configuration is described in more detail by Weinzierl et al. (2009) and Minikin et al. (2003). Although measurements and model consider different modal size ranges, the qualitative agreement is relatively good for the accumulation and coarse modes, and simulated accumulation mode particle concentrations are of the same order as observed. The measurements show rather sharp concentration gradients for all modes around 2500 m altitude, which are not represented by the model. Simulated gradients are considerably weaker for the accumulation and coarse modes, and not represented at all for the Aitken mode. The relatively coarse vertical resolution around this altitude (∼750 m) probably contributes to spurious mixing of aerosol and its precursors between the BL and the free troposphere.

It must be remarked that, although the comparison shown in Fig. 6 is not spatially and temporally consistent, the meteorological conditions were relatively homogeneous and constant over a large part of NW Europe in this period, especially after 6 May. Therefore, the comparison can be considered at least qualitatively representative for Cabauw. A total of three aerosol concentration profiles ranging between the surface and 10 km altitude were measured near Cabauw, on 6, 8, and 21 May. We compared these with the corresponding simulated profiles, with highly similar results as Figure 6, indicating that the BL mixing inaccuracies in the model are a large-scale phenomenon during these specific meteorological conditions.

4 Aerosol, humidity and AOT in selected periods

For a better understanding of the contribution of aerosol properties and RH to AOT three periods are examined in more detail, i.e., the relatively dry period between 7–12 May, the moist period between 22–26 May and the dust event between 27–30 May. Table 1 shows the average AERONET and simulated AOT for these periods, and the simulated contributions from the soluble and insoluble accumulation and coarse modes. Simulated values are filtered for clouds (see Sect. 3.1), otherwise all available simulation and observational data have been used in the calculation. Table 1 indicates that the model underestimates AOT in the dry period by 30%, and overestimates AOT in the moist period by 15% and in the dust period by 80%. AOT is dominated by the contribution from the soluble accumulation mode in the dry and moist periods. In the dust period the soluble and insoluble coarse modes contribute about 70% of the AOT, which is also expressed in a relatively small AE (Fig. 2b). The simulated Aitken mode contribution to AOT is negligible.

Table 1. Observed and simulated AOT and simulated contributions from relevant modes in the dry, moist and dust periods.

	AERONET	ECHAM	ECHAM soluble		ECHAM insoluble	
	AOT	AOT	accum	coarse	accum	coarse
dry	0.183	0.132	0.124	0.006	0.000	0.000
moist	0.402	0.469	0.448	0.014	0.000	0.007
dust	0.500	0.909	0.246	0.206	0.036	0.417

The three periods are further compared in Fig. 7 with time-averaged profiles for particle number concentrations, sulfate, RH, the accumulation mode median wet radius, the scattering coefficient μ_s (defined as the optical thickness per unit length) and the normalized cumulative (surface-to-TOA) AOT for cloud-free conditions. Simulated Aitken mode particle concentrations are relatively similar for the three periods, between 3000–4000 cm^{-3} at the surface to 1000–3000 cm^{-3} above 500 m (Fig. 7a), reflecting continuous emissions of primary particles and precursor gases in the Cabauw grid point. Accumulation mode concentrations are also similar, except for a local maximum at ∼2200 m during the moist period which is probably associated with synoptic scale advection of pollution (Fig. 7b). Surface particle concentrations maximize in the dry period. Coarse mode concentrations are relatively small in the dry and moist periods, and large during the dust period (cf. Table 1), maximizing between 2 and 6 km altitude (Fig. 7c). The model places about 60% of the total dust burden in this period below 2500 m altitude.

Aerosol sulfate concentrations are relatively small in the dry period (Fig. 7d). In the moist period sulfate maximizes at 2200 m altitude coinciding with the maximum in the accumulation mode particle concentration and humidity. This sulfate originates mostly from in-cloud chemical processes in aerosol water associated with activated modes, simulated as described by Roelofs et al. (2006). The model also associates significant sulfate amounts with the dust plume that reaches Cabauw at the end of the month. During transport across Europe the dusty air mixes with pollution and dust particles below 3000 m are processed through deposition of sulfuric acid.

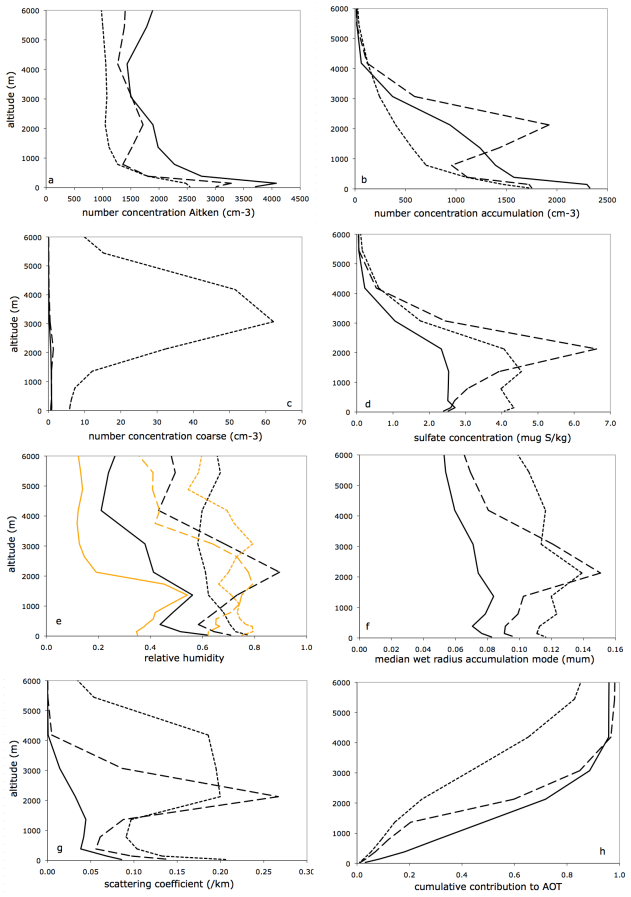

Fig. 7. Simulated profiles of number concentrations of **(a)** the Aitken, **(b)** accumulation, and **(c)** coarse mode aerosol (kg^{-1}) , and of **(d)** aerosol sulfate ($\mu g\,S\,kg^{-1}$), **(e)** RH (sonde measurements in orange), **(f)** median wet radius of the soluble accumulation mode (μm), **(g)** the scattering coefficient (km^{-1}) and **(h)** the scaled cumulative optical thickness profile, for the dry (7–12 May, solid line), moist (22–26 May, dashed) and dust periods (27–30 May, dotted).

Sonde measurements of temperature and humidity at Cabauw were performed in the morning, at noon and in the late afternoon. Figure 7e shows average observed RH profiles as well as simulated daytime averaged RH profiles. The variability of RH in the BL derived from the sonde measurements performed during IMPACT is of the order of 0.1, 0.2 and 0.15 for the dry, moist and dust periods, respectively. In the dry period simulated RH ranges from 0.55 at the surface to 0.4 at 2000 m. In the moist period simulated RH below 1500 m altitude is somewhat smaller than observed, but above 2000 m altitude it is consistently larger, on average up to ∼0.9 compared to 0.8 (observed) at 2000 m. This discrepancy may be partly due to sub-grid scale variability of RH which affects AOT (Bian et al., 2009). Aerosol swelling strongly increases with increasing RH for RH >90%, so the overestimation may have contributed to the overestimation of AOT (Table 1). In the dust period simulated RH at the surface is relatively high, 0.8, and decreases to ∼0.6 in the dust plume at 3000 m. RH is smaller than observed especially at this altitude, which may be a result of inaccurate mixing between dusty and clear air masses at the edges of the dust plume.

Simulated RH profiles display similar discrepancies compared to the observations as the simulated Aitken and accumulation mode concentration profiles (Fig. 6). In the dry period the simulated surface RH is larger than observed, which is expressed in an overestimation of IWV (Fig. 3c). Also, in the dry and the moist periods the model simulates a sharp inversion of RH at ∼400 m altitude that is not observed, possibly associated with insufficient mixing between the surface layer and the rest of the boundary layer. Additionally, the observed RH gradient at the top of the BL is sharper than in the model. This indicates that the simulated mixing between the BL and the free troposphere is more efficient than in reality, leading to excess moistening of the free troposphere.

Influenced by RH and particulate sulfate, the median wet radius of the accumulation mode (Fig. 7f) is larger in the moist and dust periods than in the dry period. Figure 7g shows the simulated scattering coefficient μ_s. Absorption in the simulation is of minor importance and will be neglected here. The scattering coefficient μ_s maximizes in the moist period, $0.25\,km^{-1}$ at ∼2000 m altitude. During the dust period also insoluble modes and the coarse mode contribute to μ_s (see Table 1) and large values are calculated close to the surface and above 2000 m. Total attenuated backscatter measurements from the Cloud-Aerosol Lidar and Infrared Pathfinder Satellite Observation (CALIPSO; http://www-calipso.larc.nasa.gov) that passed Cabauw in this period at a distance of ∼200 km, show that the aerosol resides predominantly below ∼2 km in the dry and moist periods and below ∼7 km in the dust period, consistent with our simulation.

Integrating μ_s from the surface upward and dividing by AOT yields a normalized cumulative AOT profile (Fig. 7h). The profiles show that meteorological conditions strongly influence the contribution of aerosol from different tropospheric altitudes to the column AOT. In the dry period the column AOT is dominated by the BL. About 60% of AOT is contributed by aerosol residing between 250 and 2000 m, with the remainder equally divided above and below. In the moist period 60% of the AOT derives from aerosol residing between 1500 and 2500 m where RH exceeds 90%. In the dust period, however, about 80% of AOT originates from altitudes above 2000 m. On average, the contribution of the boundary layer below 2000 m, where most anthropogenic aerosol resides, is ∼80% for the dry period, ∼60% for the moist period and ∼20% for the dust period.

4.1 Dry period, 7–12 May

In the dry period observed AOT ranges between 0.1 and 0.4 (Fig. 2a). On 7 and 8 May AOT minimizes at noon, and

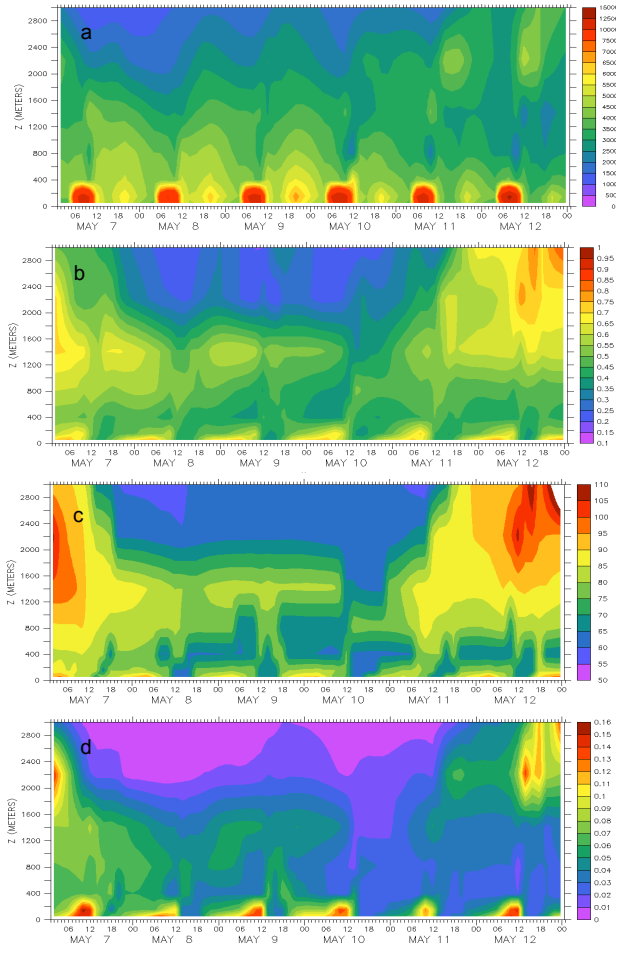

Fig. 8. **(a)** Fine mode particle concentration (cm^{-3}), **(b)** RH, **(c)** median wet radius of the soluble accumulation mode (nm), and **(d)** the scattering coefficient (km^{-1}) simulated for the dry period (7–13 May).

on 9–11 May AOT is increasing throughout the day. Simulated AOT is smaller than observed and does not display a distinct diurnal variability. To better understand the discrepancies between model and observations we examine the simulated fine mode particle concentration N_f, RH, the median wet radius of the accumulation mode r, and the scattering coefficient μ_s in the lower troposphere between 7–12 May (Fig. 8). Below 500 m the model simulates a relatively strong daily variability for N_f (Fig. 8a). In the morning, particle concentrations increase due to new particle formation as the intensity of sunlight and photochemical activity increases, in qualitative agreement with observed particle concentrations at the surface (Fig. 3b). The concentration decreases again after a few hours as result of the lifting of the boundary layer top, and dry convective transport carries particles upward to ∼1800 m. A second concentration maximum at the surface occurs around 20:00 h.

RH at the surface increases during the night to ∼75%, it decreases again during the morning to 40% and increases again in the evening (Fig. 8b). The wet radius r has a daily cycle varying between 65 nm and 95 nm at the surface (Fig. 8c). Taking into account that the simulated sulfate burden varies less than 20% (Fig. 5a), we conclude that the variability in r is dominated by RH. The relatively strong contribution by humidity in early morning is probably a contributing factor to the finding of Schaap et al. (2009) that the correlation between AERONET AOT (reflecting both dry aerosol matter and aerosol water) and surface $PM_{2.5}$ (reflecting only dry matter) is better at noon than in the morning. A weaker daily RH cycle with a similar pattern is simulated in the relatively humid layer between 1200 and 1800 m. This may be a result of vertical mixing but the layer also displays a synoptic scale variability with decreasing RH between 7–10 May and increasing RH after that. Large values of μ_s associated with relatively large RH are simulated in the boundary layer above 1000 m on 7 May and above 1500 m on 12 May. Here, μ_s appears to be correlated with r (and therefore RH) rather than with N_f (Fig. 8d). Values of μ_s in the lowest 400 m of the BL maximize in the morning due to relatively large particle number concentrations and RH. μ_s decreases rapidly towards noon and increases again in the early evening. The simulated behavior below 400 m mimics the variability in AOT observed by AERONET. However, the model atmosphere below 400 m contributes only about 20% to the total simulated AOT (Fig. 7h). it can be expected that more efficient mixing, through turbulence or dry convection, will improve simulated particle concentration and RH profiles and yield a column AOT in better agreement with the observations.

4.2 Moist and dust periods, 22–30 May

Relatively few measurements are available for 25–27 May due to occurrence of clouds and precipitation. Observed AOT varies between 0.2 and 1.4 (Fig. 2a). Simulated AOT agrees reasonably well with AERONET between 23–26 May, but exceeds AERONET values after 27 May. This may partly be due to overestimation of the atmospheric dust burden (Fig. 4). In addition, the absorptive properties of dust considered in ECHAM5-HAM are relatively small compared to other estimates and model studies (Stier et al., 2005) and this may have contributed to the discrepancy between modelled and observed AOT.

Figure 9 shows fine mode particle concentration N_f, RH, r and μ_s for 22–30 May. On 22–24 May particle concentrations below 400 m altitude show a qualitatively similar pattern as in the dry period (Fig. 9a). High concentrations are simulated between 1800 and 2500 m altitude. We remark that, on average, particle concentrations are of the same order of magnitude as in the dry period in the simulation as well as observed. However, Table 1 shows that simulated (observed) AOT in the moist period is larger by a factor of 3.5 (2.2) than in the dry period. This difference is due to RH

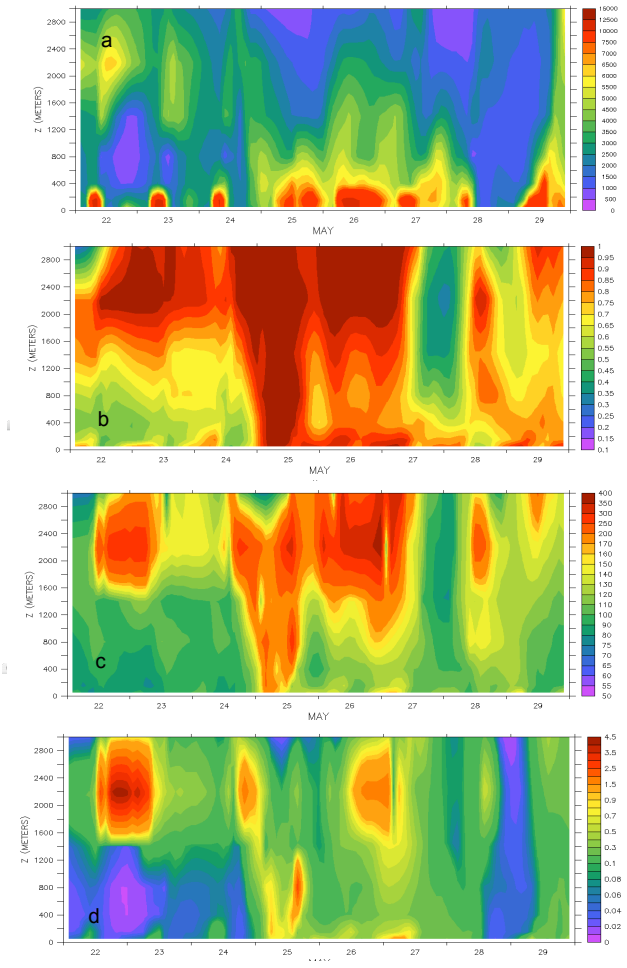

Fig. 9. **(a)** Fine mode particle concentration (cm^{-3}), **(b)** RH, **(c)** median wet radius of the soluble accumulation mode (nm), and **(d)** the scattering coefficient (km^{-1}) simulated for the moist (22–26 May) and dust periods (27–30 May).

(Fig. 9b). Although in the night of 22–23 May the lower BL was relatively dry, clouds occurred in the upper BL. Clouds were also present in the night of 24 May, and precipitating clouds the following days, so that on 25 May a large fraction of fine mode particles is washed out from the upper BL. The median wet radius (Fig. 9c) and μ_s (Fig. 9d) again correlate well with RH, and μ_s is considerably larger than in the dry period. In the evening of 27 May the air above 400 m becomes relatively dry and fine mode particle concentrations over Cabauw decrease considerably as Saharan dust is advected. The period 27–30 May is influenced by more complicated meteorology and brings a brief intermezzo of moister, relatively clean and dustless air from Atlantic origin in the second half of 28 May, leading to a relatively small μ_s and a minimum AOT in the night of 28 May (Fig. 2a).

4.3 Sensitivity study

The observations indicate that the aerosol contains more than sufficient ammonium to completely neutralize sulfate. To investigate the potential influence of ammonium and nitrate on AOT we performed an additional simulation in which a ten-fold efficiency of dissolution of nitrate is assumed (see Sect. 2), and aerosol ammonium is scaled accordingly. Figure 10 shows that with this assumption the simulated concentrations and diurnal cycle of nitrate and ammonium are approximately consistent with observations from ICG-2 Jülich in the dry period. Note that a similar daily aerosol nitrate cycle and good correlation with RH has been observed in an urban background location near London (UK) (Dall'Osto et al., 2009; their Fig. 6).

The uptake of nitric acid and ammonia by the particles enhances their hygroscopicity, and this leads to additional water uptake. In the dry period when RH maximizes in the night the simulated wet accumulation mode radius reaches values up to ∼110 nm, significantly larger than 95 nm simulated in the base case simulation (see Sect. 4.1). As a result, the simulated average AOT in this period increases from 0.132 to 0.150 (+14%). The effect is stronger on relatively humid days. For example, in the morning of 27 May the simulated wet accumulation mode radius at the surface is ∼275 nm compared to 180 nm in the base case simulation. In the moist period the computed AOT increases on average from 0.469 to 0.602 (+30%). On the other hand in the dust period when unsoluble aerosol is abundant AOT increases only mildly as result of the uptake, from 0.909 to 0.914 (+0.5%). The results from this sensitivity study are corroborated by simulations with a column aerosol-cloud model with explicit inorganic chemistry including ammonium nitrate formation (Derksen et al., 2010). This study shows that RH influences AOT in various ways, not only directly via aerosol water but also indirectly through a positive feedback between the amount of aerosol water and the uptake of nitric acid and ammonia from the gas phase. In addition, organic matter may play a significant role. In a sensitivity simulation with an organic solubility of 10% instead of 50%, the amount of aerosol water was significantly smaller than in the base case, while AOT was smaller by approximately 14% both in the dry and in the moist period. The effect on the aerosol wet size suggests that the solubility of the aerosol organic matter can thus influence the aerosol uptake of nitric acid and ammonia as suggested by Ming and Russell (2004).

5 Summary and discussion

We use the coupled aerosol-climate model ECHAM5-HAM, extended with a cloud activation and cloud chemistry scheme, in a nudged version to simulate the evolution of aerosol chemical and optical properties during the intensive aerosol-cloud measurement campaign IMPACT at Cabauw

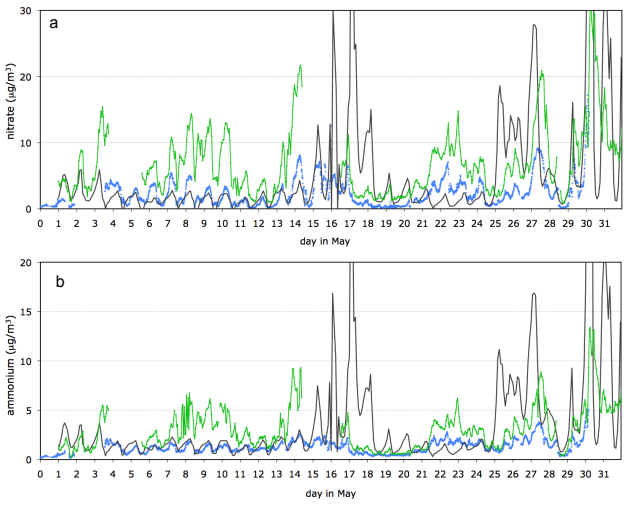

Fig. 10. Observed (blue, green; see Fig. 5) and simulated (black) concentrations (µg/m^3) of **(a)** nitrate, and **(b)** ammonium for the sensitivity study.

(the Netherlands) in May 2008. The observation period consists of relatively dry and moist periods and concludes with days characterized by advection of Saharan dust. The meteorology is represented adequately on synoptic scale, but the wind direction shows some discrepancies compared to observations while simulated IWV is larger than observed by 10–20%. The total simulated aerosol mass at the surface is about half the observed PM_{10} during most of the month, mainly due to neglect of explicit nitric acid and ammonia chemistry in the model. The dust burden over Cabauw after 25 May is overestimated. Simulated particle concentrations and concentrations of aerosol sulfate and organics are of the same order of magnitude as observed at the surface although relatively large discrepancies, up to a factor of three, occur during relatively humid conditions.

For validation, we compared simulated AOT with measurements from the AERONET network. We found that L1.5 (cloud-filtered) and L2.0 (cloud-filtered and quality-assured) data are relatively similar between 4–12 May when conditions are relatively dry, but in the second half of the month, especially after 26 May when Saharan dust is advected into the area, L2.0 contains only few data compared to L1.5. The L1.5 data in our opinion contain valuable information not present in L2.0. They reflect, for example, the strong variations in AOT and AE caused by rapid changes in wind direction in the night of 28 May, whereas L2.0 data do not. Therefore we decided to compare the simulated AOT with AERONET L1.5.

Monthly averaged values of simulated AOT are consistent within 20% with AERONET L1.5 measurements. Monthly averaged AOT, however, is not a good measure of model performance since AOT displays a relatively large variability on both synoptic and hourly/diurnal scales. The model underpredicts AOT by ∼30% when the atmosphere is relatively dry, and overpredicts AOT by ∼15% under relatively moist conditions. Discrepancies between simulated and observed moisture and particle concentration profiles suggest that inadequate BL mixing may be partly responsible. In the dry period the upward mixing during daytime of aerosol and humidity from the surface appears too weak. Further, the transport of aerosol, aerosol precursors and humidity from the upper BL to the free troposphere appears to be overestimated. This may have caused the discrepancies between simulated and observed Aitken mode particle concentrations in the BL and the free troposphere. Simulated profiles of accumulation and coarse mode particle concentrations are in better agreement with the observations. It may be expected that with a more realistic representation of BL dynamics with a less permeable BL top and realistic vertical mixing within the BL, the diurnal cycle of RH and particle concentrations will probably be expressed more prominently in AOT.

We analyzed and compared days with relatively dry and moist conditions. Aerosol dry mass and particle concentrations are of comparable magnitude in both periods while AOT differs by a factor of 2.2 in the observations, or 3.5 in the model. Further, the relative contribution of different atmospheric altitudes to AOT is different, and depends largely on the RH vertical profile. In the moist period the humid upper BL between 1500 and 2500 m altitude contributes relatively strongly to AOT while in the dry period the contribution is distributed more or less evenly below 2500 m altitude. This strongly suggests that the variability of RH dominates the variability of AOT on synoptic scales during IMPACT, rather than particle concentration and aerosol hygroscopicity. However, the strongly RH-dependent exchange of trace species between the gaseous and the aerosol phase may play an additional significant role. In the northwest European region atmospheric concentrations of nitric acid and ammonia are relatively high. A simulation with realistic concentrations demonstrates that the diurnal variability of RH induces cycling of these species between the gas phase and the aerosol, which further influences the aerosol water uptake. This enhances AOT further, in our study up to 30%. Aerosol organic matter co-determines the aerosol water uptake to a significant extent, and thus may further influence the uptake of ammonia and nitric acid. Consequently, realistic representation in climate models of the relation between RH, aerosol inorganic and organic soluble components, water uptake and gas-aerosol cycling of nitric acid and ammonia is required for accurate computation of AOT in the northwest European region.

Acknowledgements. We thank Sebastian Rast from the Max Planck Institute for Meteorology in Hamburg for his help with the nudging procedure. We thank SARA Reken- en Netwerkdiensten in Amsterdam for use of their supercomputer, and acknowledge the use of the Ferret program for the graphics (www.ferret.noaa.gov). We acknowledge AERONET for use of their data and their effort

in establishing and maintaining the Cabauw site. This work has been partly funded by EUCAARI (European Integrated project on Aerosol Cloud Climate and Air Quality interactions) No. 036833-2.

Edited by: B. Vogel

References

Anderson, T. L., Wu, Y., Chu, D. A., Schmid, B., Redemann, J., and Dubovik, O.: Testing the MODIS satellite retrieval of aerosol fine-mode fraction, J. Geophys. Res., 110, D18204, doi:10.1029/2005JD005978, 2005.

Andreae, M. O., Jones, C. D., and Cox, P. M.: Strong present-day cooling implies a hot future, Nature, 435, doi: 10.1038/nature03671, 2005.

Bellouin, N., Boucher, O., Haywood, J., and Reddy, M. S.: Global estimate of aerosol direct radiative forcing from satellite measurements, Nature, 438, 1138–1141, doi:10.1038/nature04348, 2005.

Bian, H., Chin, M., Rodriguez, J. M., Yu, H., Penner, J. E., and Strahan, S.: Sensitivity of aerosol optical thickness and aerosol direct radiative effect to relative humidity, Atmos. Chem. Phys., 9, 2375–2386, doi:10.5194/acp-9-2375-2009, 2009.

Canagaratna, M. R., Jayne, J. T., Jimenez, J. L., Allan, J. D., Alfarra, M. R., Zhang, Q., Onasch, T. B., Drewnick, F., Coe, H., Middlebrook, A., Delia, A., Williams, L. R., Trimborn, A. M., Northway, M. J., DeCarlo, P.F., Kolb, C. E., Davidovits, P., and Worsnop, D. R.: Chemical and microphysical characterization of ambient aerosols with the aerodyne aerosol mass spectrometer, Mass Spectrom. Rev., 26, 185–222, 2007.

Dall'Osto, M., Harrison, R. M., Coe, H., Williams, P. I., and Allan, J. D., Real time chemical characterization of local and regional nitrate aerosols, Atmos. Chem. Phys., 9, 3709–3720, doi:10.5194/acp-9-3709-2009, 2009.

Dentener, F., Kinne, S., Bond, T., Boucher, O., Cofala, J., Generoso, S., Ginoux, P., Gong, S., Hoelzemann, J., Ito, A., Marelli, L., Penner, J., Putaud, J.-P., Textor, C., Schulz, M.,van de Werf, G, and Wilson, J.: Emissions of primary aerosol and precursor gases in the years 2000 and 1750 -prescribed data-sets for AeroCom, Atmos. Chem. Phys., 6, 4321–4344, doi:10.5194/acp-6-4321-2006, 2006.

Derksen, J. W. B., Roelofs, G. J., and Röckmann, T.: Impact of ammonium nitrate chemistry on the AOT in Cabauw, The Netherlands, Atmos. Environ., submitted, 2010.

Eck, T. F., Holben, B. N., Dubovik, O., Smirnov, A., Goloub, P., Chen, H. B., Chatenet, B., Gomes, L., Zhang, X. Y., Tsay, S. C., Ji, Q., Giles, D., and Slutsker, I., Columnar aerosol optical properties at AERONET sites in central eastern Asia and aerosol transport to the tropical mid-Pacific, J. Geophys. Res., 110, D06202, doi:10.1029/2004JD005274, 2005.

Forster, P., Ramaswamy, V., Artaxo, P., Berntsen, T., Betts, R., Fahey, D. W., Haywood, J., Lean, J., Lowe, D. C., Myhre, G., Nganga, J., Prinn, R., Raga, G., Schulz, M., and van Dorland, R.: Changes in Atmospheric Constituents and in Radiative Forcing. In: Climate Change 2007: The Physical Science Basis. Contribution of WG I to the Fourth Assessment Report of the Intergovernmental Panel on Climate Change, edited by: Solomon, S., Qin, D., Manning, M., Chen, Z., Marquis, M., Averyt, K. B., Tignor, M., and Miller, H. L., Cambridge University Press, Cambridge, UK and New York, NY, USA, 2007.

Jeong, M. J., Li, Z., Andrews, E., and Tsay, S.-C.: Effect of aerosol humidification on the column aerosol optical thickness over the Atmospheric Radiation Measurement Southern Great Plains site, J. Geophys. Res., 112, D10202, doi:10.1029/2006JD007176, 2007.

Kaufman, Y. J., Tanré, D., and Boucher, O.: A satellite view of aerosols in the climate system, Nature, 419, 215–223, 2002.

Kaufman, Y. J., Boucher, O., Tanré, D., Chin, M., Remer, L. A., and Takemura, T.: Aerosol anthropogenic component estimated from satellite data, Geophys. Res. Lett., 32, L17804, doi:10.1029/2005GL023125, 2005.

Khlystov A., Kos, G. P. A., ten Brink, H. M., Kruisz, C., and Berner, A.: Activation properties of ambient aerosol in The Netherlands, Atmos. Environ., 30, 3281–3290, 1996.

Kulmala, M., Asmi, A., Lappalainen, H. K., Carslaw, K. S., Pöschl, U., Baltensperger, U., Hov, Ø., Brenguier, J.-L., Pandis, S. N., Facchini, M. C., Hansson, H.-C., Wiedensohler, A., and O'Dowd, C. D.: Introduction: European Integrated Project on Aerosol Cloud Climate and Air Quality interactions (EUCAARI) – integrating aerosol research from nano to global scales, Atmos. Chem. Phys., 9, 2825–2841, doi:10.5194/acp-9-2825-2009, 2009.

Kusmierczyk-Michulec, J., De Leeuw, G., and Moerman, M. M.: Physical and optical aerosol properties at the Dutch North Sea coast based on AERONET observations, Atmos. Chem. Phys., 7, 3481–3495, doi:10.5194/acp-7-3481-2007, 2007.

Lohmann, U. and Roeckner, E.: Design and performance of a new cloud microphysics scheme developed for the ECHAM4 general circulation model, Clim. Dynam., 12, 557–572, 1996.

Lohmann, U. and Feichter, J.: Global indirect aerosol effects: a review, Atmos. Chem. Phys., 5, 715–737, doi:10.5194/acp-5-715-2005, 2005.

Lohmann, U., Quaas, J., Kinne, S., and Feichter, J., Different approaches for constraining global climate models of the anthropogenic indirect aerosol effect, Bull. Amer. Meteor. Soc., 88, 243–249, doi:10.1175/BAMS-88-2-243, 2007.

Ming, Y. and Russell, L. M., Organic aerosol effects on fog droplet spectra, J. Geophys. Res., 109, D10206, doi:10.1029/2003JD004427, 2004.

Minikin, A., Petzold, A., Ström, J., Krejci, R., Seifert, M., Schlager, H., van Velthoven, P., and Schumann, U.: Aircraft observations of the upper tropospheric fine particle aerosol in the northern and southern hemispheres at midlatitudes, Geophys. Res. Lett., 30(10), 1503, doi:10.1029/2002GL016458, 2003.

Myhre, G., Grini, A., and Metzger, S.: Modelling of nitrate and ammonium-containing aerosols in presence of sea salt, Atmos. Chem. Phys., 6, 4809–4821, doi:10.5194/acp-6-4809-2006, 2006.

Myhre, G.: Consistency between satellite-derived and modeled estimates of the direct aerosol effect, Science, 325, 187–190, doi:10.1126/science.1174461, 2009.

Penner, J. E., Quaas, J., Storelvmo, T., Takemura, T., Boucher, O., Guo, H., Kirkevåg, A., Kristjánsson, J. E., and Seland, Ø.: Model intercomparison of indirect aerosol effects, Atmos. Chem. Phys., 6, 3391–3405, doi:10.5194/acp-6-3391-2006, 2006.

Quaas, J., Boucher, O., Bellouin, N., and Kinne, S.: Satellite-based estimate of the direct and indirect aerosol climate forcing, J. Geo-

phys. Res., 113, D05204, doi:10.1029/2007JD008962, 2008.

Quaas, J., Ming, Y., Menon, S., Takemura, T., Wang, M., Penner, J. E., Gettelman, A., Lohmann, U., Bellouin, N., Boucher, O., Sayer, A. M., Thomas, G. E., McComiskey, A., Feingold, G., Hoose, C., Kristjánsson, J. E., Liu, X., Balkanski, Y., Donner, L. J., Ginoux, P. A., Stier, P., Feichter, J., Sednev, I., Bauer, S. E., Koch, D., Grainger, R. G., Kirkevåg, A., Iversen, T., Seland, Ø., Easter, R., Ghan, S. J., Rasch, P. J., Morrison, H., Lamarque, J.-F., Iacono, M. J., Kinne, S., and Schulz, M.: Aerosol indirect effects – general circulation model intercomparison and evaluation with satellite data, Atmos. Chem. Phys., 9, 8697–8717, doi:10.5194/acp-9-8697-2009, 2009.

Roelofs, G. J., Stier, P., Feichter, J., Vignati, E., and Wilson, J.: Aerosol activation and cloud processing in the global aerosol-climate model ECHAM5-HAM, Atmos. Chem. Phys., 6, 2389–2399, doi:10.5194/acp-6-2389-2006, 2006.

Roelofs, G. J.: A GCM study of organic matter in marine aerosol and its potential contribution to cloud drop activation, Atmos. Chem. Phys., 8, 709–719, 2008, http://www.atmos-chem-phys.net/8/709/2008/.

Roelofs, G. J. and Kamphuis, V.: Cloud processing, cloud evaporation and Angström exponent, Atmos. Chem. Phys., 9, 71–80, doi:10.5194/acp-9-71-2009, 2009.

Schaap, M., Apituley, A., Timmermans, R. M. A., Koelemeijer, R. B. A., and de Leeuw, G.: Exploring the relation between aerosol optical depth and $PM_{2.5}$ at Cabauw, the Netherlands, Atmos. Chem. Phys., 9, 909–925, doi:10.5194/acp-9-909-2009, 2009.

Schuster, G. L., Dubovik, O., and Holben, B. N.: Angström exponent and bimodal aerosol size distributions, J. Geophys. Res., 111, D07207, doi:10.1029/2005JD006328, 2006.

Stier, P., Feichter, J., Kinne, S., Kloster, S., Vignati, E., Wilson, J., Ganzeveld, L., Tegen, I., Werner, M., Balkanski, Y., Schulz, M., and Boucher, O.: The aerosol-climate model ECHAM5-HAM, Atmos. Chem. Phys., 1125–1156, doi:10.5194/acp-5-1125-2005, 2005.

Textor, C., Schulz, M., Guibert, S., Kinne, S., Balkanski, Y., Bauer, S., Berntsen, T., Berglen, T., Boucher, O., Chin, M., Dentener, F., Diehl, T., Easter, R., Feichter, H., Fillmore, D., Ghan, S., Ginoux, P., Gong, S., Grini, A., Hendricks, J., Horowitz, L., Huang, P., Isaksen, I., Iversen, I., Kloster, S., Koch, D., Kirkevåg, A., Kristjansson, J. E., Krol, M., Lauer, A., Lamarque, J. F., Liu, X., Montanaro, V., Myhre, G., Penner, J., Pitari, G., Reddy, S., Seland, Ø., Stier, P., Takemura, T., and Tie, X.: Analysis and quantification of the diversities of aerosol life cycles within AeroCom, Atmos. Chem. Phys., 6, 1777–1813, doi:10.5194/acp-6-1777-2006, 2006.

Vignati, E., Wilson, J. and Stier, P.: M7: An efficient size-resolved aerosol microphysics module for large-scale aerosol transport models, J. Geophys. Res., 109, D22202, doi:10.1029/2003JD004485, 2004.

Wehner, B., Siebert, H., Ansmann, A., Ditas, F., Seifert, P., Stratmann, F., Wiedensohler, A., Apituley, A., Shaw, R. A., Manninen, H. E., and Kulmala, M.: Observations of turbulence-induced new particle formation in the residual layer, Atmos. Chem. Phys., 10, 4319–4330, doi:10.5194/acp-10-4319-2010, 2010.

Weinzierl, B., Petzold, A., Esselborn, M., Wirth, M., Rasp, K., Kandler, K., Schütz, L., Koepke, P. and Fiebig, M.: Airborne measurements of dust layer properties, particle size distribution and mixing state of Saharan dust during SAMUM 2006, Tellus B, 61, 96–117. doi:10.1111/j.1600-0889.2008.00392.x, 2009.

Wilson, J., Cuvelier, C., and Raes, F.: A modeling study of global mixed aerosol fields, J. Geophys. Res., 106, 34081–34108, doi:10.1029/2000JD000198, 2001.